Novel Smart Wearable Sensors Based on PVDF Reinforced With CNTs for Human Motion Monitoring

Víctor Díaz Mena, Xoan Xosé F. Sánchez Romate, David Martínez Díaz, María Sánchez Martínez, and Alejandro Ureña Fernández

***Abstract*—Wearable strain sensors based on poly(vinylidene fluoride-co-hexafluoropropylene) (PVDF-HFP) reinforced with carbon nanotubes (CNTs) dispersed with Triton surfactant by solvent casting are proposed. The analysis of the electrical response shows that the conductivity increases with CNT content, as expected, whereas the addition of a high content of surfactant is more efficient at low CNT contents as it forms a more efficient electrical network. An ac analysis with electrochemical impedance spectroscopy was carried out, where the variation in R_{int}/R_{tunnel} ratio with CNT and surfactant content was analyzed. This ratio shows when the electrical pathway is saturated and the electrical transport occurs mainly through the aggregates, or when the tunneling mechanism starts to take relevance. Electromechanical analysis under tensile loading shows that the sensitivity increases with decreasing the CNT content, reaching gauge factor (GF) values of around 10^4 at 80%–90% strain level, higher than most of the research found in the literature. Furthermore, the electrical response under cycling loading shows similar peak and base values between consecutive cycles in a medium-term response, highlighting the robustness of the sensors. Finally, the sensors are subjected to a proof-of-concept test for finger and elbow movement monitoring, where a good agreement between the electrical and mechanical response is observed, demonstrating the applicability of the proposed materials for monitoring medium and large human movements.**

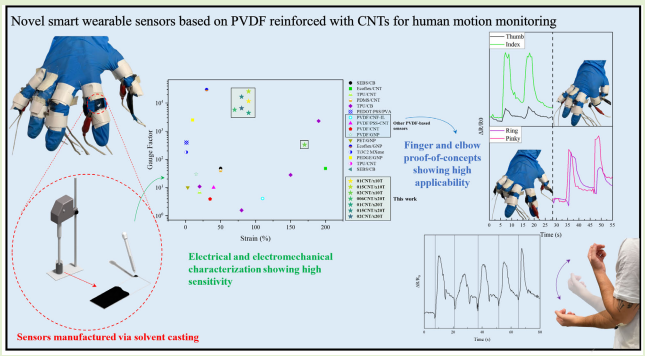

***Index Terms*— Electrical properties, healthcare monitoring, nanoparticles, smart materials, strain sensors.**

Manuscript received 19 February 2024; revised 15 March 2024; accepted 18 March 2024. Date of publication 2 April 2024; date of current version 15 May 2024. This work was supported in part by the Agencia Estatal de Investigación of the Spanish Government Project MULTISENS, under Grant PID2022-136636OB-I00; and in part by the Young Researchers IMPULSO Program through the Universidad Rey Juan Carlos, SMARTSENS under Grant 2986. The associate editor coordinating the review of this article and approving it for publication was Prof. Anindya Nag. *(Corresponding author: Víctor Díaz Mena.)*

This work involved human subjects or animals in its research. The authors confirm that all human/animal subject research procedures and protocols are exempt from review board approval.

Víctor Díaz Mena, Xoan Xosé F. Sánchez Romate, and David Martínez Díaz are with the Materials Science and Engineering Area, Escuela Superior de Ciencias Experimentales y Tecnología, Universidad Rey Juan Carlos, 28933 Madrid, Spain (e-mail: victor.diaz@urjc.es).

María Sánchez Martínez and Alejandro Ureña Fernández are with the Materials Science and Engineering Area, Escuela Superior de Ciencias Experimentales y Tecnología, and the Instituto de Investigación de Tecnologías para la Sostenibilidad, Universidad Rey Juan Carlos, 28933 Madrid, Spain.

This article has supplementary downloadable material available at https://doi.org/10.1109/JSEN.2024.3381550, provided by the authors.

Digital Object Identifier 10.1109/JSEN.2024.3381550

I. Introduction

THANKS to the advances in medicine achieved in recent decades, there are diagnostic tools for almost any disease or analyte that a doctor wants to measure or detect in a patient. In this regard, in recent years, the use of strain wearable sensors for human monitoring has attracted considerable attention due to factors such as affordability and ergonomics, and the capability of continuously monitoring the biometrics of an individual in a noninvasive or minimally invasive way. This makes it possible to detect small physiological changes from baseline values over time and provides a new tool for medical personnel to continuously obtain health-quality data from their patients [1].

The strain wearable sensors can capture the motion state and posture of different parts of the human body, which is crucial for rehabilitation therapy applications [2], [3], [4], [5], [6], [7]. In this regard, piezoresistive sensors have been widely explored due to their low fabrication costs and ease of signal acquisition [8], [9].

The wearable sensors must adapt to the nonplanar surface of the human body. Conventional strain sensors based on metal or semiconductors are becoming obsolete due to their poor stretchability, in addition to other factors such as their limited sensitivity (with a gauge factor (GF) of 2–3 at every strain level). In this regard, composite materials based on flexible polymeric matrices have emerged as the most suitable replacement [10]. These typically consist of three main components [11]: flexible matrix, active sensing element, and electrodes. The material matrix must be chosen carefully to provide good flexibility, stretchability, and long-term reliability. The active element is defined as the reinforcement that will grant the electrical behavior, which defines the sensing mechanism. The electrodes must be well-designed for acquiring a robust and stable electrical signal.

The selection of the polymer and reinforcement, coupled with an appropriate processing route, is challenging from a materials' science point of view [12]. The main materials used for this purpose are polymers such as PDMS [13], PVDF [14], [15], [16], [17], PET [18], [19], and TPU [20], [21], [22].

Poly(vinylidene fluoride-co-hexafluoropropylene) (PVDF-HFP) is one of the main copolymers of PVDF, showing the lowest Young modulus, dielectric constant, and price. Its high chemical and thermal tolerance only increases its attractiveness for sensing applications [23]. The main advantage of using thermoplastic polymers as matrix relies on the capability to recycle the sensor by melting down, thus representing an interesting variant for both scientific research and application at the industrial level [24].

When adding conductive nanoparticles inside a dielectric polymer, its electrical conductivity is described by percolation theory in the vicinity of insulator–conductor transition [25], where the formation of electrical networks once a critical volume fraction, called the percolation threshold, is reached. The most studied active materials as nanofillers for these types of sensors have been carbon derivatives (graphene [26], [27], [28], [29], carbon nanotubes (CNTs) [30], [31], [33], carbon black [34], [35], [36]), and metallic nanoparticles [8]. Among these, carbon derivatives are the ones that have been more widely investigated. CNTs have attracted much attention because the percolation threshold of typical CNT-filled conducting nanocomposites is less than 1.0 wt.% due to its inherent high conductivity and high aspect ratios [37], [38], [39].

However, the use of the CNTs as nano-reinforcement may be limited due to some difficulties associated with the dispersion of entangled CNTs during processing and the high cost of CNTs. As the surface area of a particle increases, so does the Van der Waals attractive forces between them this, together with the high flexibility of the CNTs, increases the possibility of entanglement and close packing [40]. This issue can be avoided by selecting an appropriate dispersion route when manufacturing the nanocomposites [41]. One of the main methods used is the addition of a surfactant when dispersing the CNTs [40]. Rastogi et al. [42] carried out a comparison study of CNT dispersion using four different surfactants (Triton X-100, Tween 20, Tween 80, and sodium dodecyl sulfate), where the Triton X-100 showed the best-dispersing power due to its benzene ring.

In this research, novel wearable piezoresistive sensors based on a thermoplastic matrix (PVDF-HFP) with CNTs and low percolation threshold for body motion applications are developed.

First, in Section II, the sensor manufacturing process by solvent casting and sonication will be described. Here, several conditions of CNTs and surfactant content (Triton X-100) will be manufactured to study the effect of both on the sensor's response.

In Section III, the characterization of the sensors in terms of microstructure, electrical properties, and electromechanical response will be carried out. This will be carried out by a dc and ac electrical conductivity analysis and by strain sensing tests under tensile conditions and will focus on the differences found with the CNTs percentages added and the content of surfactant. One condition will be selected or a final step in characterization based on a proof-of-concept test of different body movements.

Finally, Section IV will summarize the main results obtained and the conclusion extracted about the wearable sensors manufactured and their possible future application in human health applications.

II. Materials and Methods

A. Film Preparation

PVDF-HFP, as received from Byosynth,[1] was dissolved in N,N-dimethylformamide (DMF), purchased from SigmaAldrich,[1] to form a PVDF-HFP solution with a ratio of 1 g of PVDF-HFP:10-mL DMF. The solution was continuously stirred using a magnetic stirrer for 2 h at 300 rpm at room temperature. Multiwall CNTs (MWCNTs or CNTs hereinafter) NC7000, supplied by Nanocyl[1] (95% purity), were added to the solution in different concentrations (0.06, 0.1, 0.15, and 0.2 wt.%) with Triton X-100 as a surfactant purchased from DOW,[1] which was added 10 and 20 times the mass of CNT for each concentration mentioned to explore its effect on the dispersion of CNTs and thus on the created electrical network.

The dispersion of CNTs in the PVDF solution was carried out by ultrasonication technique in a Hielscher Ultrasonic Processor UP400ST machine at 0.5 pulse cycles and 50% amplitude for 30 min.

Before depositing the solution, each substrate was cleaned with acetone in an ultrasonic bath for 10 min. Then, ∼4 mL of the solution was deposited on the flat glass substrates, as shown in Fig. 1. Then, heat treatment was applied at 90 °C for 1 h to evaporate the remaining solvent. Both the substrate and the solvent evaporation treatment were selected according to the literature [43], [44], [45]. The nanocomposite films with dimensions 70 × 25 × 0.08 mm^3 were extracted from the substrate after solvent evaporation treatment. All manufactured films are summarized in Table I with the nomenclature used for each one.

B. Characterization

1) Microstructural Characterization: For the microstructural characterization, a Leica DMR optical microscope (OM) with

[1]Registered trademark.

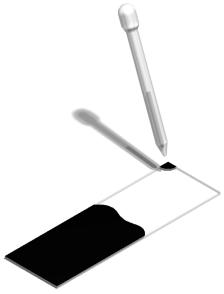

Fig. 1. Visual scheme of the solution deposition on cleaned glass substrate process.

TABLE I
SUMMARY OF NOMENCLATURE FOR THE DIFFERENT NANOCOMPOSITE FILMS PREPARED

Sample nomenclature	wt. % CNTs	Triton condition
006CNT/x10T	0.06	x10
01CNT/x10T	0.1	
015CNT/x10T	0.15	
02CNT/x10T	0.2	
006CNT/x20T	0.06	x20
01CNT/x20T	0.1	
015CNT/x20T	0.15	
02CNT/x20T	0.2	

ImagePro Plus image processing software was used. Due to the transparency of the PVDF-HFP and the low thickness of the manufactured sample probes, transmission mode was carried out on the films to analyze the dispersion of CNTs inside the matrix.

2) Electrical Characterization: Volumetric conductivity in direct current was evaluated using a KEITHLEY Source Meter Unit instrument (Series 2400 SourceMeter[1] 1100 V-to-1 μV voltage output range, 0.012% basic measure accuracy with 61/2-digit resolution). The electrical resistance was determined by calculating the slope of the current–voltage characteristic curve within the range of 0–100 V in the case of an ohmic behavior, and three samples were tested per condition. For the test, two electrodes based on adhesive copper foil and copper wires were placed on the edges of each sample.

AC tests were performed by electrical impedance spectroscopy (EIS) by using an AUTOLAB potentiostat (PGSTAT302N station, with −10- to 10-V output range, ± 0.2% ± 2 mV and ± 0.2% ± 0.2% of voltage and current accuracy, 0.3 μV of potential resolution, and 1 MHz of maximum bandwidth) equipped with Nova 2.1 software for analysis with equivalent circuits. Measurements were taken between two electrodes in an arrangement like that of dc testing. The real and imaginary parts of electrical impedance ($Z^* = Z' + jZ''$) were measured in the frequency range of 0.1–10^5 Hz at 0.3-V voltage amplitude. Both configurations for dc and ac measurements are shown in Fig. 2 along with a detailed schematic of the electrodes.

C. Strain Monitoring Tests

Quasi-static and cyclic tensile tests were performed on a Zwick universal tensile machine with a 500-N load cell (Materials Testing Machines ProLine Z100 with test loads from 500 N to 100 kN, a measurement ranges up to 165% of Fmax). For these tests, six specimens of each condition were tested. For the cyclic tests, a speed of 10 mm/min was used, reaching a value of 5% and 10% strain for 200 cycles. This last type of test was performed to analyze the repeatability of the measurement, a critical parameter when evaluating the robustness of strain sensors.

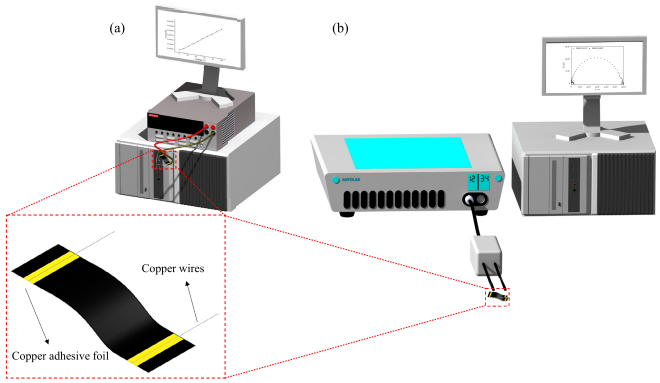

Fig. 2. Visual schemes of the setups for (a) dc and (b) ac electrical behavior tests with a detailed image of the electrodes on the sample.

Simultaneously to both mechanical tests, the electrical response was recorded, by measuring the electrical resistance between the two copper wire electrodes with an Agilent test unit at an acquisition frequency of 10 Hz (34410A multimeter with a 100 mV–1000 V output range, 100 Ω–1 GΩ measuring range, and 3 Hz–300 kHz acquisition frequency range). In this sense, the GF, defined as the change in normalized resistance divided by the applied strain, was calculated for each condition to evaluate the most sensitive sensor

$$\mathrm{GF} = \frac{\Delta R/R_0}{\varepsilon} \tag{1}$$

where $\Delta R/R_0$ is the change of the normalized electrical resistance, recorded by the Agilent hardware, and ε is the applied mechanical strain.

D. Proof-of-Concept Tests

To evaluate the sensors developed during this study, several human motion monitoring tests were performed. On the one hand, the performance of the strain sensor was evaluated in terms of finger motion monitoring. In this case, a nitrile glove with sensors attached to each finger was used for the proof.

On the other hand, an elbow motion monitoring test was also performed by placing the sensor directly on the skin. In this case, several stretching and bending movements of the elbow were conducted to evaluate the robustness of the sensors. During the test, the electrical resistance variation was recorded using the Agilent 34410A module. The main author of the research paper gave his full consent to the development of these tests on the abovementioned parts of his body.

III. RESULTS AND DISCUSSION

In this section, first, an analysis of the dispersion of the CNTs inside the polymer matrix is carried out. Then, the

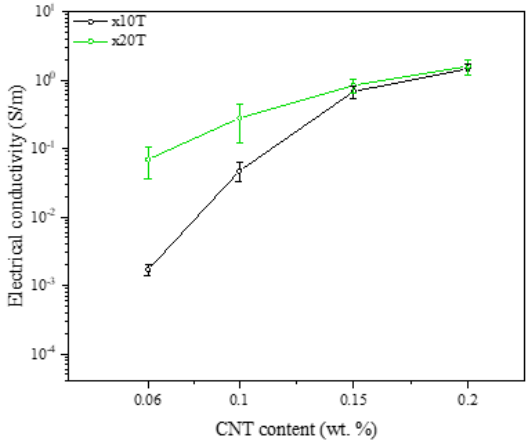

Fig. 3. DC conductivities as a function of CNT contents.

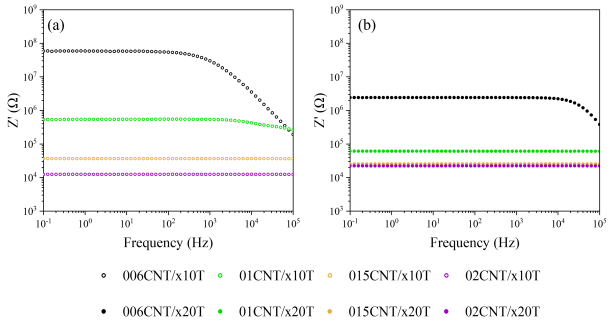

Fig. 4. Z' plots as a function of ac frequency. (a) $\times$10T and (b) $\times$20T samples.

electrical properties of PVDF-HFP/CNT films are studied by dc and ac measurements to better understand the effect of CNT dispersion and interactions on the electronic transport of these materials. Finally, their strain sensing capabilities are fully characterized by quasi-static and cyclic tests, and a proof-of-concept as wearable sensors is performed.

A. Microstructural Analysis

Fig. S1 shows the dispersion of CNTs for each condition. Here, as the CNT content increases, the number of CNT aggregates also increases for both $\times$10 and $\times$20 Triton surfactant contents, as expected. For the lower CNT contents (0.06 and 0.1 wt.%), the amount of surfactant needed to coat the entire CNT surface is less, and its addition helps to homogenize the CNT distribution, leading to less CNT entanglement.

Furthermore, the increased Triton content implies more effective dispersion of CNTs at lower nanoparticle contents [42], [46], helping to form CNT pathways throughout the material. However, at higher CNT contents, differences between the CNT dispersion with the amount of Triton are less prevalent.

B. Analysis of Electrical Properties

1) DC Electrical Conductivity Tests: Fig. 3. shows the dc electrical conductivity values for the different CNT and Triton contents. First, it can be concluded that all the percentages of CNTs studied in this research have electrical conductivity, which means that with the production route carried out, a lower percolation threshold has been achieved than in other studies with this copolymer [23].

It can be observed that, at low CNT contents (below 0.15 wt.%), the samples with the highest amount of surfactant ($\times$20T) show the highest electrical conductivities. However, the opposite trend is observed at higher CNT contents, where the higher electrical conductivity was achieved with the lowest amount of surfactant ($\times$10T). Therefore, it can be concluded that the surfactant plays a crucial role in the electrical properties of the manufactured films.

More specifically, at low nanofiller contents, CNTs are usually present in the form of small, isolated aggregates [47], as already mentioned in the microstructural analysis. As discussed, the more Triton is added for these lower contents of CNTs, the more electrical pathways are formed, leading to achieving a better electrical conductivity result.

However, at high nanofiller contents, it was mentioned that Triton content hardly affects the dispersion of the CNTs, a higher Triton content would be necessary to observe a crucial difference between the dispersion. This is the reason why, for 0.15 and 0.2 wt.% of CNTs, the electrical conductivity barely varies between the Triton conditions studied.

Considering the geometry of the sensor samples and the distance between contacts, electrical conductivities of 1.46 ± 0.27 and 1.60 ± 0.39 S/m were measured for 0.2CNT $\times$10 and $\times$20 of Triton, respectively.

2) AC Conductivity Analysis: For a better understanding of the electrical transport mechanisms inside the PVDF-HFP/CNT nanocomposite, an analysis of the complex impedance response was carried out. In this sense, Fig. 4. summarizes the variation of the real part (Z') of the impedance as a function of the ac frequency.

It can be observed that the samples with higher amounts of CNTs present a frequency-independent behavior of the real part for the measured frequency range. However, the samples with 0.06 for both surfactant conditions, $\times$10T and $\times$20T, and with 0.1 wt.% CNTs for $\times$10T present a frequency-dependent behavior of the real part of the impedance at high frequencies.

This has been observed in other studies [48] and is explained by the fact that at higher CNT contents, the charge density carrier is high enough to travel through the material without any phase shift between the current and the voltage. However, at lower CNT contents, the charge carrier density is lower, and therefore, at high frequencies, a lag is observed between applied voltage and current, which manifests in a variation of the real part with frequency.

Fig. 5 shows the Nyquist plots of the different PVDF-HFP/CNT samples showing the variation of the real (Z') and imaginary (Z'') parts as a function of frequency. The dots show the data points extracted from the tests and the lines are the fit performed with equivalent circuits. It can be noticed that the EIS behavior of the samples with a frequency-dependent electrical response is shown in a semicircle or a composition of different semicircles [Fig. 5(a) and (b)] in the Nyquist plot. This behavior has been observed in previous studies using different graphitic nanofillers: CNTs and GNPs [48], [49]. More specifically, the variation of the real and imaginary

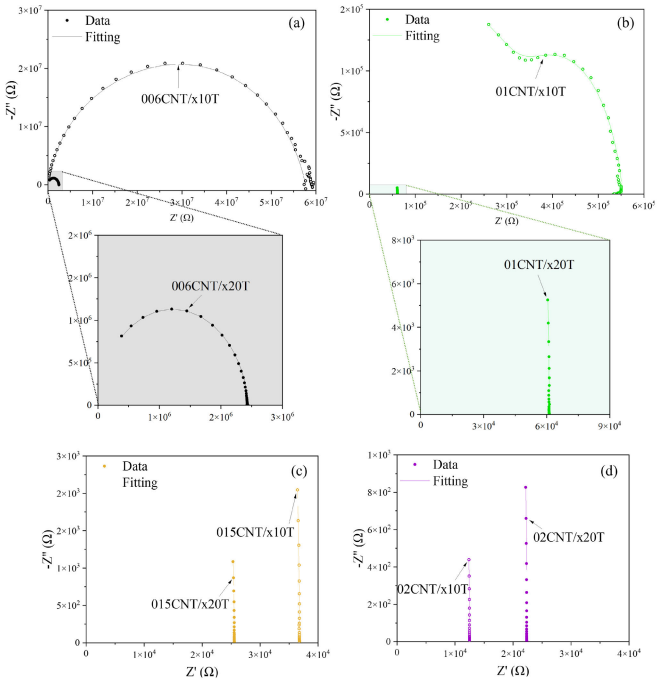

Fig. 5. Nyquist plots of (a) 0.06, (b) 0.1, (c) 0.15, and (d) 0.2 wt.% CNT samples where the solid symbols denote the ×20T and the hollowed ones the ×10T samples.

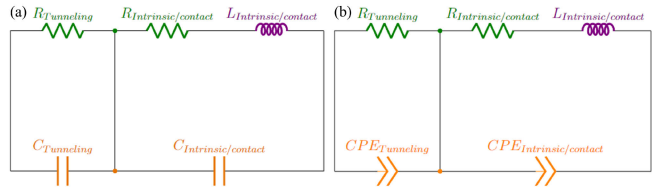

Fig. 6. Scheme of the equivalent circuit used for modeling the electrical behavior with the frequency where (a) is the equivalent circuit with capacitors and (b) is the equivalent circuit using CPEs instead of capacitors.

parts can be modeled by an equivalent electrical circuit that can provide a more detailed view of the electrical transport mechanisms in this type of material.

This electrical circuit consists of a series of resistors in parallel with a capacitor (*RC*) and a resistor in series with an inductance, and both in parallel with a capacitor element (LRC), as shown in the schematic of Fig. 5. The *RC* element denotes electrical transport due to the tunneling effect between neighboring nanoparticles and the LRC one denotes electrical transport due to the intrinsic conductivity of the CNTs and conduction mechanisms through the aggregates. More specifically, in a previous study, capacitance terms were often replaced by constant phase elements (CPEs). A CPE is a nonideal resistive–capacitive element that denotes energy dissipation through the resistive part, unlike a pure capacitor, which denotes effective conservation [50], [51]. Its impedance is defined by $Z = 1/(Q_o(j\omega)^n)$. A value of $n = 0$ denotes a pure resistor, whereas a value of $n = 1$ represents a pure capacitor.

Therefore, the correlation between the experimental measurements and the fitted data by using the equivalent circuit of Fig. 6(b) is also shown in the plots of Fig. 5. There is a

TABLE II
ADJUSTMENT PARAMETERS (IN OHMS) FROM EQUIVALENT CIRCUIT MODELING SAMPLE BEHAVIOR

	R_{in} (Ω)		R_{tunnel} (Ω)	
	x10T	**x20T**	**x10T**	**x20T**
0.06 CNT	4.77E+07	1.34E+06	1.00E+07	1.10E+06
0.1 CNT	2.30E+05	1.17E+04	3.19E+05	4.95E+04
0.15 CNT	1.00E+04	1.50E+03	2.68E+04	2.40E+04
0.2 CNT	5.00E+03	5.00E+03	7.49E+03	1.73E+04
	R_{in}/R_{tunnel}			
	x10T		**x20T**	
0.06 CNT	4.77E+00		1.22E+00	
0.1 CNT	7.21E-01		2.36E-01	
0.15 CNT	3.73E-01		6.25E-02	
0.2 CNT	6.68E-01		2.89E-01	

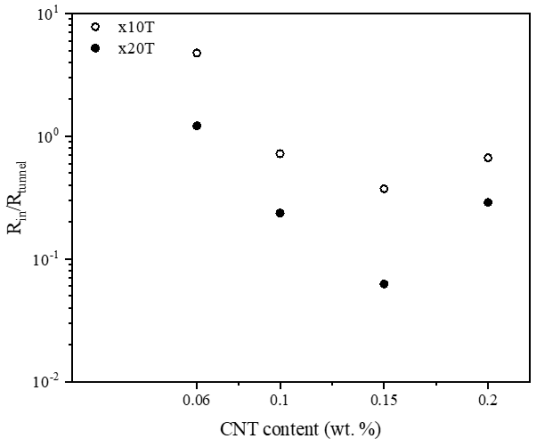

Fig. 7. Correlation between the electrical resistance associated with the intrinsic/contact mechanisms and the tunneling effect for the different conditions.

good agreement between the measurements and the electrical circuit fit, and therefore, it can be concluded that the proposed equivalent circuit properly captures the main electrical transport mechanisms in this type of material.

More specifically, Table II summarizes the different fitting parameters of the samples, and Fig. 7. shows the correlation between the values of the electrical resistance associated with the RCPE element (tunneling transport) and the electrical resistance associated with the LRCPE (intrinsic and contact mechanisms).

It can be observed that, at very low CNT contents (0.06 wt.%), the main conduction mechanism takes place through the aggregates, with an $R_{\text{int}}/R_{\text{tunnel}}$ ratio higher than 1. This can be explained, as discussed above in the dc analysis because CNTs tend to be in the form of small and isolated aggregates at very low nanofiller contents. An increase in the Triton content promotes a reduction of the intrinsic mechanisms due to a better dispersion of CNTs, which would explain the higher conductivity values. However, by increasing the CNT content up to 0.15 wt.%, the $R_{\text{int}}/R_{\text{tunnel}}$ ratio decreases as

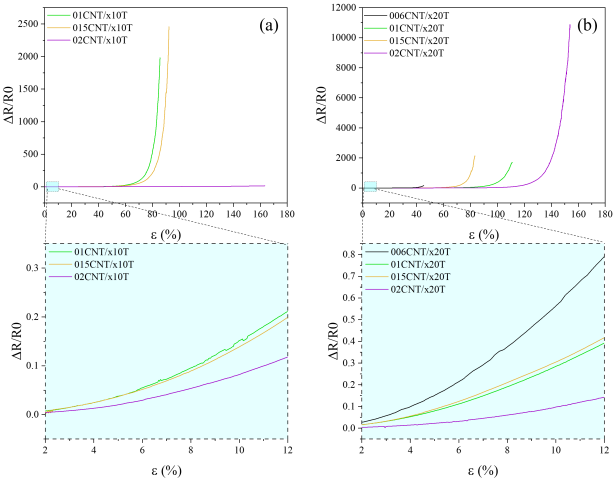

Fig. 8. Electromechanical quasi-static tensile stress tests, where the electrical response with strain is observed for each sample for (a) ×10T and (b) ×20T conditions.

multiple CNT-CNT tunneling connections are created through the nanocomposite. This is reflected in a sudden increase in electrical conductivity and a more efficient electrical network. Finally, for higher CNT contents (0.2 wt.%), new CNT-CNT contacts are formed throughout the network and intrinsic and contact mechanisms start to dominate the electrical transport, which is reflected in an increase of the R_{int}/R_{tunnel} ratio, explaining the saturation of electrical conductivity previously observed.

C. Electromechanical Tests

1) Quasi-Static Tests: Fig. 8. shows the electrical response, in terms of normalized resistance variation, with tensile stress applied during the electromechanical tests. It should be noted that the resistivity of the sample 006CNT/×10T was outside of the range of the Agilent 34410A equipment used for these tests due to its low electrical conductivity, so no electrical response was recorded during the mechanical test. The 02CNT/×10T condition did not show a very prevalent exponential response with applied strain, as it did not lose electrical contact before breakage.

The mechanical tests show an elastic behavior for all sensors up to a stress level of 20–25 MPa (yield stress) and then a constant plastic deformation up to 150%–200% strain in almost all cases. The detail of the electrical response for low strain levels is shown in the enlarged plots of Fig. 8. for each Triton condition, where a more dominant linear dependence is observed. However, as the strain level increases, the exponential effects of the variation of the electrical resistance become more dominant. When strain levels close to the loss of electrical contact are reached, the electrical resistance increases sharply, reaching values high enough that the test system is unable to register it.

Fig. 9 shows the variation of GF as a function of CNT content for both Triton conditions. The standard deviation is shown for each condition up to 40% strain, as at higher percentages the values would become meaningless as each sample tested per condition does not break at the same strain level.

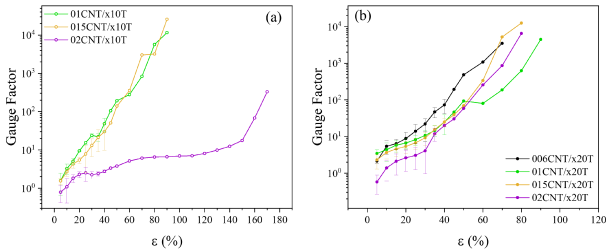

Fig. 9. GF values as a function of applied strain for (a) ×10T and (b) ×20T conditions.

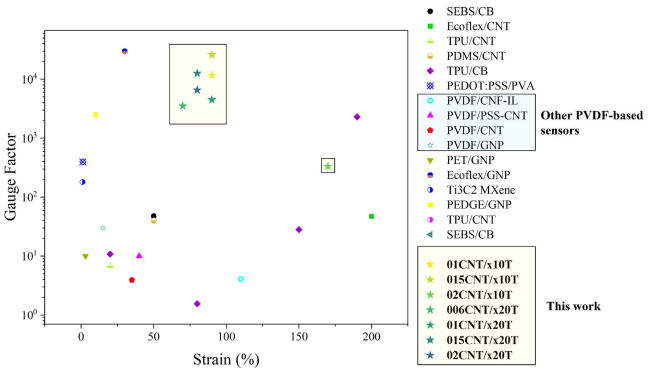

Fig. 10. Comparison of the relationships between GFs and strain values referenced in the literature and those obtained in this work.

For the ×10T condition, the maximum GF achieved is approximately 2.6 × 10^4 at 90% of strain for the 0.15 wt.% CNT condition. Here, it can be observed that lower CNT content generally gives higher GF for the same strain level. Therefore, for the same Triton content and process parameters, it can be said that the lower the CNT contents, the fewer electrical pathways are formed and the more severe effect of tunneling conductivity between isolated aggregates, resulting in an exponential variation of resistivity when the nanocomposite is deformed.

When Triton content increases, as was mentioned before with the dc and ac analysis, further disaggregation of larger agglomerates occurs. For this condition, the GF for the sample with 0.1 wt.% of CNTs has a value of about 40% for 50% deformation, while the sample with 0.06 wt.% of CNTs reaches a GF of about 1100 for the same 50% strain. This phenomenon confirms that, in this case, the amount of surfactant used in the 0.06 wt.% CNT condition is high enough to promote a well-dispersed network and, therefore, the electrical sensitivity to deformation is much higher, which is explained by the larger interparticle distance between neighboring CNTs. At this Triton content, the maximum GF is around 2.0 × 10^4 at a strain level of 110% for the 0.1 wt.% CNT condition, which highlights the effectiveness of the tunneling transport mechanisms between neighboring CNTs in this condition.

Fig. 10 shows a comparison between this work and other studies carried out by several researchers based on thermoplastic and thermoset nanocomposites, such as SEBS/CB [52], Ecoflex/CNT [53], Ecoflex/GNP [54], PDMS/CNT [55], TPU/CB [21], [35], [56], TPU/CNT [57], PVDF/CNF-IL [58], PVDF/CNT [59], [60], PVDF/GNP [15], PET/GNP [61],

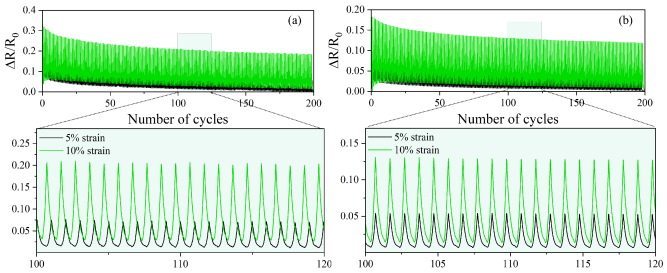

Fig. 11. Electrical response during 200 cycles for (a) 0.06CNT/×20T and (b) 0.1CNT/×10T conditions.

PEDGE/GNP [62], PEDOT:PSS/PVA [63], and Ti_3C_2 MXene [64]. The 02CNT/×10T material has the lowest GF value due to the phenomenon discussed above. All the other systems present competitive values with the Ecoflex/GNP system and well above the other studied systems.

2) Cycling Tests: Fig. 11 shows the electrical response with the number of cycles for 200 cycles under tensile conditions to study the medium-term stability of the nanocomposites. These tests were performed for the two most sensitive conditions: 0.06CNT/×20T and 0.1CNT/×10T since they would be the most suitable for strain detection purposes due to their high GF at low strains. Two facts should be noted. On the one hand, an increase in both peak and baseline electrical resistance values in the first cycle. This has been previously observed [65] and it is correlated to the irreversibility of the electrical paths generated between neighboring nanoparticles after the first stretch-compressive cycle. However, after this increase, the electrical response between consecutive cycles does not change significantly over the 200 cycles, as can be seen in the magnified images in Fig. 11 with an increased sensitivity (defined as the variation of the electrical resistance in a single cycle) with applied strain, as expected.

The electrical drift or hysteresis in the cyclic tests is 0.015 (5%) and 0.008 (10%) for the 0.1CNT/×10T. For the 0.06CNT/×20T conditions, the respective values are 0.041 (5%) and 0.011 (10%). These values have been calculated by subtracting the final $\Delta R/R_0$ measured (200 cycles) from the initial $\Delta R/R_0$ value at the first cycle. Fig. 12 shows the $\Delta R/R_0$ versus displacement curves for the two conditions. The mentioned hysteresis value is marked in each graph in a yellow box. It can be concluded that the proposed sensors present a very robust electrical response under dynamic loads.

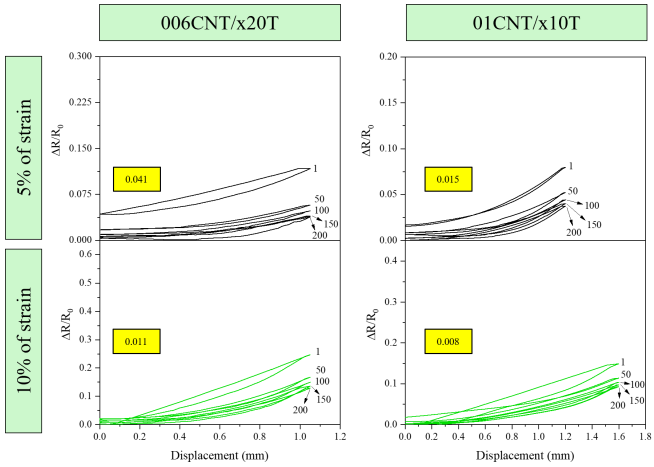

Fig. 12. Hysteresis loop for the two conditions tested under cyclic tests. Five cycles are presented for each condition.

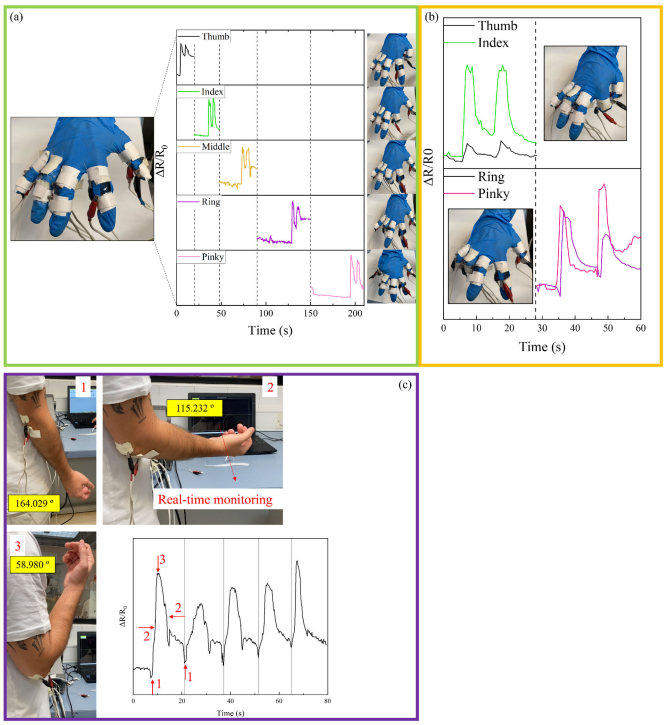

Fig. 13. Electrical response of each sensor during the proof-of-concept testing for (a) independent movement of each finger, (b) movement of two fingers at a time, and (c) elbow movements.

D. Proof-of-Concept Analysis

As a last step as mentioned above, two proofs of concept were carried out to emulate a possible application of these sensors in the healthcare sector.

Fig. 13 shows both proofs of concept. Fig. 13(a) shows the electrical response associated with the movement of each finger during the first proof, where each finger was bent twice consecutively. For these tests, the 0.1CNT/×10T sensor was selected, as it showed high sensitivity, especially at low and medium strain levels with a suitable noise level. Here, it can be observed that the electrical response is in good agreement with the mechanical one, with an increase in the electrical resistance in each finger while bent. Since the change of the electrical resistance depends on the strain level of each finger, it can be observed that the thumb has the smallest variation of electrical resistance variation due to the smaller deformation associated with the movement of this finger compared with the rest. Fig. 13(b) also shows the electrical response when a finger combination of movements is carried out, where the electrical resistance changes according to the different finger displacements. Therefore, it is possible to monitor certain finger signs with the proposed sensors.

Fig. 13(c) shows the electrical response for the elbow tests, where the three different movements are marked in the figure

and shown with the corresponding image. The sequence of the movements was performed five times during the analysis. In this case, it can be observed that the electrical resistance increases as the elbow is bent, such as the finger movements. More specifically, it is possible to obtain simultaneous tracking of the elbow movement, as seen in the images of Fig. 13(c), where marked point 1 corresponds to the relaxed posture, point 2 corresponds to 90° elbow flexion, and point 3 corresponds to full elbow flexion. This sequence was repeated five times to demonstrate the robustness of the proposed sensor, and the results showed that they can correctly monitor medium-to-large human movements.

IV. Conclusion

Flexible strain sensors based on PVDF reinforced with CNTs with very robust electrical response have been proposed. First, the electrical response under different CNT and surfactant conditions was analyzed, to properly understand the main electrical transport mechanisms. It is observed that the electrical conductivity increases with CNT content, as expected, due to the higher number of electrical pathways formed inside the nanocomposite. As for the effect of surfactant, it can be elucidated that higher surfactant contents improve CNT dispersion at low nanofiller contents by generating a more efficient electrical network, while the opposite effect is found at high CNT contents, where high amounts of surfactant can negatively affect the electrical transport between neighboring nanoparticles.

Electromechanical tests under tensile conditions showed a higher sensitivity, defined by the GF, with decreasing the CNT content, due to a higher prevalence of tunneling mechanisms between neighboring nanoparticles, whereas the electrical transport is dominated by intrinsic and contact mechanisms at high CNT contents, which are less sensitive to mechanical strain. The maximum GF values were found around 104 at a strain level of 80–90 demonstrating an enormous sensitivity to large deformations.

Analysis of the electromechanical properties under cycling loading showed a very similar electrical response between consecutive cycles throughout the test, with very low variations in peak and baseline electrical resistance values, demonstrating the high robustness of the manufactured sensors.

Finally, the proof-of-concept tests for fingers and elbow movements were successfully carried out, with a good agreement between the recorded electrical response and the human movements, demonstrating the high applicability of the proposed sensors for monitoring deformations of medium and large strain levels.

References

[1] J. Heikenfeld et al., "Wearable sensors: Modalities, challenges, and prospects," *Lab Chip*, vol. 18, no. 2, pp. 217–248, 2018, doi: 10.1039/c7lc00914c.

[2] D. Lu et al., "Highly sensitive fabric strain sensor with double-layer conductive networks for joint rehabilitation therapy," *Compos. Sci. Technol.*, vol. 230, Nov. 2022, Art. no. 109778, doi: 10.1016/j.compscitech.2022.109778.

[3] D. S. Wood et al., "Accurate prediction of knee angles during open-chain rehabilitation exercises using a wearable array of nanocomposite stretch sensors," *Sensors*, vol. 22, no. 7, p. 2499, Mar. 2022, doi: 10.3390/s22072499.

[4] G. Li et al., "Wide strain range and high sensitivity sandwich structure CNTs/AgNWs/CNTs/TPU strain sensors for human motion detection," *Sens. Actuators A, Phys.*, vol. 366, Feb. 2024, Art. no. 114998, doi: 10.1016/j.sna.2023.114998.

[5] L. Lin et al., "Superhydrophobic and wearable TPU based nanofiber strain sensor with outstanding sensitivity for high-quality body motion monitoring," *Chem. Eng. J.*, vol. 419, Sep. 2021, Art. no. 129513, doi: 10.1016/j.cej.2021.129513.

[6] T. Pawar, S. Chaudhuri, and S. P. Duttagupta, "Body movement activity recognition for ambulatory cardiac monitoring," *IEEE Trans. Biomed. Eng.*, vol. 54, no. 5, pp. 874–882, May 2007, doi: 10.1109/TBME.2006.889186.

[7] X.-L. Xu, S.-X. Li, Y. Yang, X.-C. Sun, and H. Xia, "High-performance strain sensor for detection of human motion and subtle strain by facile fabrication," *Measurement*, vol. 189, Feb. 2022, Art. no. 110658, doi: 10.1016/j.measurement.2021.110658.

[8] W. Chiappim, M. A. Fraga, H. Furlan, D. C. Ardiles, and R. S. Pessoa, "The status and perspectives of nanostructured materials and fabrication processes for wearable piezoresistive sensors," *Microsyst. Technol.*, vol. 28, no. 7, pp. 1561–1580, Jul. 2022, doi: 10.1007/s00542-022-05269-w.

[9] J. Li, L. Fang, B. Sun, X. Li, and S. H. Kang, "Review—Recent progress in flexible and stretchable piezoresistive sensors and their applications," *J. Electrochem. Soc.*, vol. 167, no. 3, Jan. 2020, Art. no. 037561, doi: 10.1149/1945-7111/ab6828.

[10] L. Li, L. Han, H. Hu, and R. Zhang, "A review on polymers and their composites for flexible electronics," *Mater. Adv.*, vol. 4, no. 3, pp. 726–746, Feb. 2023, doi: 10.1039/d2ma00940d.

[11] L. Xie et al., "Intelligent wearable devices based on nanomaterials and nanostructures for healthcare," *Nanoscale*, vol. 15, no. 2, pp. 405–433, Jan. 2023, doi: 10.1039/d2nr04551f.

[12] M. Hassan et al., "Significance of flexible substrates for wearable and implantable devices: Recent advances and perspectives," *Adv. Mater. Technol.*, vol. 7, 2022, Art. no. 2100773, doi: 10.1002/admt.202100773.

[13] A. del Bosque, X. Sánchez-Romate, M. Sánchez, and A. Ureña, "Wearable sensors based on graphene nanoplatelets reinforced polydimethylsiloxane for human motion monitoring: Analysis of crack propagation and cycling load monitoring," *Chemosensors*, vol. 10, no. 2, p. 75, Feb. 2022, doi: 10.3390/chemosensors10020075.

[14] Y. Tanaka, D. P. Nguyen, T. Fukuda, and A. Sano, "Wearable skin vibration sensor using a PVDF film," in *Proc. IEEE World Haptics Conf. (WHC)*, 2015, pp. 146–151, doi: 10.1109/WHC.2015.7177705.

[15] H. C. Bidsorkhi, A. G. D'Aloia, A. Tamburrano, G. De Bellis, and M. S. Sarto, "Waterproof graphene-PVDF wearable strain sensors for movement detection in smart gloves," *Sensors*, vol. 21, no. 16, p. 5277, Aug. 2021, doi: 10.3390/s21165277.

[16] M. Jing et al., "Porous AgNWs/poly(vinylidene fluoride) composite-based flexible piezoresistive sensor with high sensitivity and wide pressure ranges," *ACS Appl. Mater. Intererface*, vol. 14, no. 49, pp. 55119–55129, Dec. 2022, doi: 10.1021/acsami.2c17879.

[17] Y. Miao et al., "Preparation of multi-axial compressible 3D PVDF nanofibre/graphene wearable composites sensor sponge and application of integrated sensor," *Sens. Actuators A, Phys.*, vol. 342, Aug. 2022, Art. no. 113648, doi: 10.1016/j.sna.2022.113648.

[18] Q. A. Alsulami, S. Wageh, A. A. Al-Ghamdi, R. M. H. Bilal, and M. A. Saeed, "A tunable and wearable dual-band metamaterial absorber based on polyethylene terephthalate (PET) substrate for sensing applications," *Polymers*, vol. 14, no. 21, p. 4503, Oct. 2022, doi: 10.3390/polym14214503.

[19] X. Zhao, Q. Hua, R. Yu, Y. Zhang, and C. Pan, "Flexible, stretchable and wearable multifunctional sensor array as artificial electronic skin for static and dynamic strain mapping," *Adv. Electron. Mater.*, vol. 1, 2015, Art. no. 1500142, doi: 10.1002/aelm.201500142.

[20] T. Chen et al., "A novel flexible piezoresistive sensor using superelastic fabric coated with highly durable SEBS/TPU/CB/CNF nanocomposite for detection of human motions," *Compos. Sci. Technol.*, vol. 227, Aug. 2022, Art. no. 109563, doi: 10.1016/j.compscitech.2022.109563.

[21] X. Yue et al., "Highly stretchable and durable fiber-shaped strain sensor with porous core-sheath structure for human motion monitoring," *Compos. Sci. Technol.*, vol. 189, Mar. 2020, Art. no. 108038, doi: 10.1016/j.compscitech.2020.108038.

[22] S. Li, R. Li, O. G. González, T. Chen, and X. Xiao, "Highly sensitive and flexible piezoresistive sensor based on c-MWCNTs decorated TPU electrospun fibrous network for human motion detection," *Compos. Sci. Technol.*, vol. 203, Feb. 2021, Art. no. 108617, doi: 10.1016/j.compscitech.2020.108617.

[23] J. Vicente, P. Costa, S. Lanceros-Mendez, J. M. Abete, and A. Iturrospe, "Electromechanical properties of PVDF-based polymers reinforced with nanocarbonaceous fillers for pressure sensing applications," *Materials*, vol. 12, no. 21, p. 3545, Oct. 2019, doi: 10.3390/ma12213545.

[24] S. Coiai, E. Passaglia, A. Pucci, and G. Ruggeri, "Nanocomposites based on thermoplastic polymers and functional nanofiller for sensor applications," *Materials*, vol. 8, no. 6, pp. 3377–3427, Jun. 2015, doi: 10.3390/ma8063377.

[25] İ. Mutlay and L. B. Tudoran, "Percolation behavior of electrically conductive graphene nanoplatelets/polymer nanocomposites: Theory and experiment," *Fullerenes, Nanotubes Carbon Nanostruct.*, vol. 22, no. 5, pp. 413–433, Mar. 2014, doi: 10.1080/1536383x.2012.684186.

[26] Q. Zheng, J.-H. Lee, X. Shen, X. Chen, and J.-K. Kim, "Graphene-based wearable piezoresistive physical sensors," *Mater. Today*, vol. 36, pp. 158–179, Jun. 2020, doi: 10.1016/j.mattod.2019.12.004.

[27] K.-Y. Chen, Y.-T. Xu, Y. Zhao, J.-K. Li, X.-P. Wang, and L.-T. Qu, "Recent progress in graphene-based wearable piezoresistive sensors: From 1D to 3D device geometries," *Nano Mater. Sci.*, vol. 5, no. 3, pp. 247–264, Sep. 2023, doi: 10.1016/j.nanoms.2021.11.003.

[28] C. Hong, S. Yuan, W.-B. Chen, X. Chen, J. Yu, and A. Chen, "Fabrication and verification of vertical graphene-based strain sensor," *Measurement*, vol. 218, Aug. 2023, Art. no. 113265, doi: 10.1016/j.measurement.2023.113265.

[29] R. Zhang, J. Jiang, and W. Wu, "Wearable chemical sensors based on 2D materials for healthcare applications," *Nanoscale*, vol. 15, no. 7, pp. 3079–3105, Feb. 2023, doi: 10.1039/d2nr05447g.

[30] W. Obitayo and T. Liu, "A review: Carbon nanotube-based piezoresistive strain sensors," *J. Sensors*, vol. 2012, pp. 1–15, Jan. 2012, doi: 10.1155/2012/652438.

[31] R. Atoche-Enseñat et al., "A smart tactile sensing system based on carbon nanotube/polypropylene composites for wearable applications," *IEEE Sensors J.*, vol. 23, no. 3, pp. 2948–2955, Feb. 2023, doi: 10.1109/JSEN.2022.3229232.

[32] G. K. Rajini and D. Maji, "Cost-effective, disposable, flexible, and printable MWCNT-based wearable sensor for human body temperature monitoring," *IEEE Sensors J.*, vol. 22, no. 17, pp. 16756–16763, Sep. 2022, doi: 10.1109/JSEN.2021.3088466.

[33] A. Palumbo, Z. Li, and E.-H. Yang, "Trends on carbon nanotube-based flexible and wearable sensors via electrochemical and mechanical stimuli: A review," *IEEE Sensors J.*, vol. 22, no. 21, pp. 20102–20125, Nov. 2022, doi: 10.1109/JSEN.2022.3198847.

[34] W. Zhai et al., "Multifunctional flexible carbon black/polydimethylsiloxane piezoresistive sensor with ultrahigh linear range, excellent durability and oil/water separation capability," *Chem. Eng. J.*, vol. 372, pp. 373–382, Sep. 2019, doi: 10.1016/j.cej.2019.04.142.

[35] Y. Zhai et al., "Flexible and wearable carbon black/thermoplastic polyurethane foam with a pinnate-veined aligned porous structure for multifunctional piezoresistive sensors," *Chem. Eng. J.*, vol. 382, Feb. 2020, Art. no. 122985, doi: 10.1016/j.cej.2019.122985.

[36] H. Zhu et al., "Flexible, high-sensitive and multifunctional wearable sensor based on the dual bioinspired spinosum microstructure of carbon nanotube/carbon black-coated polydimethylsiloxane film," *Measurement*, vol. 207, Feb. 2023, Art. no. 112402, doi: 10.1016/j.measurement.2022.112402.

[37] X. Lu, Y. Liu, L. Pichon, D. He, O. Dubrunfaut, and J. Bai, "Effective electrical conductivity of CNT/polymer nanocomposites," in *Proc. Int. Symp. Electromagn. Compat.*, Sep. 2020, pp. 1–4, doi: 10.1109/EMCEUROPE48519.2020.9245805.

[38] Z.-H. Tang, Y.-Q. Li, P. Huang, H. Wang, N. Hu, and S.-Y. Fu, "Comprehensive evaluation of the piezoresistive behavior of carbon nanotube-based composite strain sensors," *Compos. Sci. Technol.*, vol. 208, May 2021, Art. no. 108761, doi: 10.1016/j.compscitech.2021.108761.

[39] J. Li, P. C. Ma, W. S. Chow, C. K. To, B. Z. Tang, and J. Kim, "Correlations between percolation threshold, dispersion state, and aspect ratio of carbon nanotubes," *Adv. Funct. Mater.*, vol. 17, no. 16, pp. 3207–3215, Nov. 2007, doi: 10.1002/adfm.200700065.

[40] L. Vaisman, H. D. Wagner, and G. Marom, "The role of surfactants in dispersion of carbon nanotubes," *Adv. Colloid Interface Sci.*, vols. 128–130, pp. 37–46, Dec. 2006, doi: 10.1016/j.cis.2006.11.007.

[41] Y. Y. Huang and E. M. Terentjev, "Dispersion of carbon nanotubes: Mixing, sonication, stabilization, and composite properties," *Polymers*, vol. 4, no. 1, pp. 275–295, Jan. 2012, doi: 10.3390/polym4010275.

[42] R. Rastogi, R. Kaushal, S. K. Tripathi, A. L. Sharma, I. Kaur, and L. M. Bharadwaj, "Comparative study of carbon nanotube dispersion using surfactants," *J. Colloid Interface Sci.*, vol. 328, no. 2, pp. 421–428, Dec. 2008, doi: 10.1016/j.jcis.2008.09.015.

[43] D. Kunwar, I. R. Vazquez, and N. Jackson, "Effects of solvents on synthesis of piezoelectric polyvinylidene fluoride trifluoroethylene thin films," *Thin Solid Films*, vol. 757, Sep. 2022, Art. no. 139414, doi: 10.1016/j.tsf.2022.139414.

[44] I. Y. Abdullah, M. Yahaya, M. H. H. Jumali, and H. M. Shanshool, "Influence of the substrate on the crystalline phase and morphology of poly (vinylidene fluoride) (PVDF) thin film," *Surf. Rev. Lett.*, vol. 23, no. 3, Jun. 2016, Art. no. 1650005, doi: 10.1142/s0218625x16500050.

[45] D. L. Chinaglia et al., "Influence of the solvent evaporation rate on the crystalline phases of solution-cast poly(vinylidene fluoride) films," *J. Appl. Polym. Sci.*, vol. 116, no. 2, pp. 785–791, Apr. 2010, doi: 10.1002/app.31488.

[46] X. F. Sánchez-Romate, A. Jiménez-Suárez, J. Molinero, M. Sánchez, A. Güemes, and A. Ureña, "Development of bonded joints using novel CNT doped adhesive films: Mechanical and electrical properties," *Int. J. Adhes. Adhesives*, vol. 86, pp. 98–104, Nov. 2018, doi: 10.1016/j.ijadhadh.2018.09.001.

[47] X. F. Sánchez-Romate et al., "Highly sensitive strain gauges with carbon nanotubes: From bulk nanocomposites to multifunctional coatings for damage sensing," *Appl. Surf. Sci.*, vol. 424, pp. 213–221, Dec. 2017, doi: 10.1016/j.apsusc.2017.03.234.

[48] T. N. Tallman and H. Hassan, "A network-centric perspective on the microscale mechanisms of complex impedance in carbon nanofiber-modified epoxy," *Composites Sci. Technol.*, vol. 181, Sep. 2019, Art. no. 107669, doi: 10.1016/j.compscitech.2019.05.026.

[49] A. D. Bosque, X. F. Sánchez-Romate, M. Sánchez, and A. Ureña, "Ultrasensitive and highly stretchable sensors for human motion monitoring made of graphene reinforced polydimethylsiloxane: Electromechanical and complex impedance sensing performance," *Carbon*, vol. 192, pp. 234–248, Jun. 2022, doi: 10.1016/j.carbon.2022.02.043.

[50] A. Lasia, "The origin of the constant phase element," *J. Phys. Chem. Lett.*, vol. 13, no. 2, pp. 580–589, Jan. 2022, doi: 10.1021/acs.jpclett.1c03782.

[51] A. Sanli, C. Müller, O. Kanoun, C. Elibol, and M. F.-X. Wagner, "Piezoresistive characterization of multi-walled carbon nanotube-epoxy based flexible strain sensitive films by impedance spectroscopy," *Compos. Sci. Technol.*, vol. 122, pp. 18–26, Jan. 2016, doi: 10.1016/j.compscitech.2015.11.012.

[52] L. Ma et al., "Carbon black/graphene nanosheet composites for three-dimensional flexible piezoresistive sensors," *ACS Appl. Nano Mater.*, vol. 5, no. 5, pp. 7142–7149, May 2022, doi: 10.1021/acsanm.2c01081.

[53] S. Ryu et al., "Extremely elastic wearable carbon nanotube fiber strain sensor for monitoring of human motion," *ACS Nano*, vol. 9, no. 6, pp. 5929–5936, Jun. 2015, doi: 10.1021/acsnano.5b00599.

[54] A. del Bosque, X. F. Sánchez-Romate, A. Gómez, M. Sánchez, and A. Ureña, "Highly stretchable strain sensors based on graphene nanoplatelet-doped ecoflex for biomedical purposes," *Sens. Actuators A, Phys.*, vol. 353, Apr. 2023, Art. no. 114249, doi: 10.1016/j.sna.2023.114249.

[55] A. D. Bosque, X. F. Sánchez-Romate, M, Sánchez, and A. Ureña, "Easy-scalable flexible sensors made of carbon nanotube-doped polydimethylsiloxane: Analysis of manufacturing conditions and proof of concept," *Sensors*, vol. 22, p. 5147, Jan. 2022, doi: 10.3390/s22145147.

[56] T. Chen et al., "Recent advances of flexible strain sensors based on conductive fillers and thermoplastic polyurethane matrixes," *ACS Appl. Polym. Mater.*, vol. 3, no. 11, pp. 5317–5338, Nov. 2021, doi: 10.1021/acsapm.1c00840.

[57] Y. Zheng et al., "Conductive thermoplastic polyurethane composites with tunable piezoresistivity by modulating the filler dimensionality for flexible strain sensors," *Compos. A, Appl. Sci. Manuf.*, vol. 101, pp. 41–49, Oct. 2017, doi: 10.1016/j.compositesa.2017.06.003.

[58] B. Prasad, F. S. Gill, V. Panwar, and G. Anoop, "Development of strain sensor using conductive poly(vinylidene fluoride) (PVDF) nanocomposite membrane reinforced with ionic liquid (IL) & carbon nanofiber (CNF)," *Compos. B, Eng.*, vol. 173, Sep. 2019, Art. no. 106990, doi: 10.1016/j.compositesb.2019.106990.

[59] V. Sankar, K. Balasubramaniam, and R. Sundara, "Insights into the effect of polymer functionalization of multiwalled carbon nanotubes in the design of flexible strain sensor," *Sens. Actuators A, Phys.*, vol. 322, May 2021, Art. no. 112605, doi: 10.1016/j.sna.2021.112605.

[60] A. Ferreira, M. T. Martínez, A. Ansón-Casaos, L. E. Gómez-Pineda, F. Vaz, and S. Lanceros-Mendez, "Relationship between electromechanical response and percolation threshold in carbon nanotube/poly(vinylidene fluoride) composites," *Carbon*, vol. 61, pp. 568–576, Sep. 2013, doi: 10.1016/j.carbon.2013.05.038.

[61] H. Tian et al., "Scalable fabrication of high-performance and flexible graphene strain sensors," *Nanoscale*, vol. 6, no. 2, pp. 699–705, 2014, doi: 10.1039/c3nr04521h.

[62] A. del Bosque et al., "Ultrasensitive flexible strain sensors based on graphene nanoplatelets doped poly(ethylene glycol) diglycidyl ether: Mask breathing monitoring for the Internet of Things," *Sens. Actuators A, Phys.*, vol. 358, Aug. 2023, Art. no. 114448, doi: 10.1016/j.sna.2023.114448.

[63] N. Liu, G. Fang, J. Wan, H. Zhou, H. Long, and X. Zhao, "Electrospun PEDOT: PSS–PVA nanofiber based ultrahigh-strain sensors with controllable electrical conductivity," *J. Mater. Chem.*, vol. 21, no. 47, p. 18962, 2011, doi: 10.1039/c1jm14491j.

[64] Y. Ma et al., "A highly flexible and sensitive piezoresistive sensor based on MXene with greatly changed interlayer distances," *Nature Commun.*, vol. 8, no. 1, p. 18, Oct. 2017, doi: 10.1038/s41467-017-01136-9.

[65] W. Li et al., "Core–Sheath fiber-based wearable strain sensor with high stretchability and sensitivity for detecting human motion," *Adv. Electron. Mater.*, vol. 7, no. 1, Jan. 2021, Art. no. 2000865, doi: 10.1002/aelm.202000865.

Víctor Díaz Mena received the B.Sc. degree in materials engineering and the M.Sc. degree in materials manufacturing technologies from Rey Juan Carlos University, Madrid, Spain, in 2021 and 2022, respectively.

He started his research in materials science and engineering at Rey Juan Carlos University. His research interests include the development of nanocomposite materials for human motion monitoring.

Xoan Xosé F. Sánchez Romate received the Ph.D. degree in aerospace engineering from the Polytechnic University of Madrid, Madrid, Spain, in 2019.

He has been an Associate Professor of Materials Science and Engineering at Rey Juan Carlos University since 2015. His research interests include the application of carbon nanoparticles to develop multifunctional composite structures and polymers with self-sensing properties.

David Martínez Díaz received the Ph.D. degree in chemical engineering from Rey Juan Carlos Uiversity, Madrid, Spain, in 2021.

He has been an Associate Professor of Materials Science and Engineering at Rey Juan Carlos University since 2021. His research interests include the development of new energy storage devices based on polymeric matrix composites with structural purposes. Moreover, he is also working on the recycling process of CFRP composite materials.

María Sánchez Martínez received the Ph.D. degree in materials science from Rey Juan Carlos University, Madrid, Spain, in 2007.

She has been a Full Professor of Materials Science and Engineering at Rey Juan Carlos University since 2022. Her research interests include the application of carbon nanoparticles to the improvement of properties and the development of new functionalities in polymers and polymeric matrix composite materials. Moreover, she develops brazing of refractory materials for their application in the future nuclear fusion reactor DEMO.

Alejandro Ureña Fernández received the Ph.D. degree in chemical sciences and European welding engineering from the Complutense University of Madrid, Madrid, Spain, in 1987.

He has been a Full Professor of Materials Science and Engineering at Rey Juan Carlos University since 2002. His research interests include two main lines the application of nanotechnology to the improvement of properties and the development of new functionalities in polymers and polymeric matrix composite materials, and the brazing of refractory materials for their application in the nuclear fusion reactor DEMO.